1098–1112 *Nucleic Acids Research, 2008, Vol. 36, No. 4* *Published online 20 December 2007*
doi:10.1093/nar/gkm1083

Loop dependence of the stability and dynamics of nucleic acid hairpins

Serguei V. Kuznetsov[1], Cha-Chi Ren[2], Sarah A. Woodson[2] and Anjum Ansari[1,3,*]

[1]Department of Physics (M/C 273), University of Illinois at Chicago, 845 W. Taylor St., Chicago, IL 60607, [2]Department of Biophysics, Johns Hopkins University, 3400 N. Charles St, Baltimore, MD 21218-2685 and [3]Department of Bioengineering (M/C 063), University of Illinois at Chicago, 845 W. Taylor St., Chicago, IL 60607, USA

Received June 19, 2007; Revised November 6, 2007; Accepted November 19, 2007

ABSTRACT

Hairpin loops are critical to the formation of nucleic acid secondary structure, and to their function. Previous studies revealed a steep dependence of single-stranded DNA (ssDNA) hairpin stability with length of the loop (L) as $\sim L^{8.5\pm0.5}$, in 100 mM NaCl, which was attributed to intraloop stacking interactions. In this article, the loop-size dependence of RNA hairpin stabilities and their folding/unfolding kinetics were monitored with laser temperature-jump spectroscopy. Our results suggest that similar mechanisms stabilize small ssDNA and RNA loops, and show that salt contributes significantly to the dependence of hairpin stability on loop size. In 2.5 mM $MgCl_2$, the stabilities of both ssDNA and RNA hairpins scale as $\sim L^{4\pm0.5}$, indicating that the intraloop interactions are weaker in the presence of Mg^{2+}. Interestingly, the folding times for ssDNA hairpins (in 100 mM NaCl) and RNA hairpins (in 2.5 mM $MgCl_2$) are similar despite differences in the salt conditions and the stem sequence, and increase similarly with loop size, $\sim L^{2.2\pm0.5}$ and $\sim L^{2.6\pm0.5}$, respectively. These results suggest that hairpins with small loops may be specifically stabilized by interactions of the Na^+ ions with the loops. The results also reinforce the idea that folding times are dominated by an entropic search for the correct nucleating conformation.

INTRODUCTION

One of the major efforts in basic biopolymer science is directed toward an understanding of the energetics and mechanisms by which single-stranded (ss) polynucleotides form their secondary and higher order structures. Hairpins, or stem–loops, are the simplest secondary structure elements. The formation of hairpins in transient ssDNA regions and their involvement in biological processes such as replication, transcription and recombination is now well documented in both prokaryotic and eukaryotic systems (1–5). In RNA molecules, hairpins serve as nucleation sites for RNA folding as well as make up a significant part of its secondary structure (6–8), and an understanding of hairpin energetics and dynamics is a starting point for our comprehension of the folding of larger RNA molecules (9–11). In addition, diverse RNA stem–loops play critical roles in RNA–protein recognition and gene regulation (12–14). The stability and relaxation dynamics of RNA hairpins are central to the operation of regulatory switches (15) and the application of small interfering RNAs (siRNAs) for targeted gene silencing (16,17).

Precise measurements of the folding times of fundamental units of secondary structure, such as hairpins, provide insights into the conformational flexibility of the ss-chains, and the nature and strength of the intrachain interactions that stabilize these structures, and test our understanding of their stability and dynamics. It has long been recognized that, at the simplest level, hairpin formation is nucleated by the formation of a loop, stabilized by a few base pairs, followed by 'zipping' of the stem (18). Kinetics measurements on short self-complementary oligomers, carried out in the early seventies using microsecond temperature-jump (T-jump) techniques based on electric discharge, revealed that hairpins with 4–6 nucleotides (nt) in the loop and <10 base pairs (bp) in the stem fold on time-scales of tens of microseconds (19–21).

Understanding the time-scales on which hairpins form requires an estimate of the time-scales for forming loops. This, in turn, requires reliable estimates of the free energy cost of loop formation, and deeper insights into the nature of the folding nucleus. In recent years, there has been a surge in hairpin folding kinetics studies using a variety of

*To whom correspondence should be addressed. Tel: +312 996 8735; Fax: +312 996 9016; Email: ansari@uic.edu
Present address:
Cha-Chi Ren, DC Public Schools, 825 N. Capitol St, Washington D.C. 20036, USA

new experimental tools, such as fluctuation correlation spectroscopy (FCS) and single-molecule FRET measurements (22–29), laser T-jump measurements (30–34), and single-molecule micromanipulation experiments (35–38). These measurements, together with computational and theoretical studies (39–44), have started to reveal the underlying complexity in the free energy landscape of even simple structures such as hairpins.

If intrachain interactions are ignored, and the ss-polynucleotide is treated like an ideal semiflexible polymer, the purely entropic conformational search time for the two ends of a ~10-nt long chain to come together is estimated to be tens of nanoseconds (31,45). This estimated time-scale for loop formation is about three orders of magnitude shorter than the observed times for hairpin formation, raising a fundamental question as to what is the rate-determining step?

The ~40 ns estimate for the end-to-end contact time for a ~10-nt loop assumes a random walk polymer with a statistical segment length of ~4 nt (31,46). However, there is mounting evidence that intrachain interactions in ss-polynucleotides that lead to nonideal behavior are nonnegligible (47–55). A dramatic illustration of this nonideal behavior came from our earlier study on the stability of ssDNA hairpins with poly(dT) or poly(dA) loops ranging from 4 to 12 bases (31,56), in which we showed that the free energy cost of loop formation scaled with the length L of the loop as $\Delta G_{\rm loop} \sim \alpha \ln(L)$, with $\alpha \approx 8.5$, significantly higher than $\alpha \approx 1.5$ expected for a random walk chain, and $\alpha \approx 2$ expected for a self-avoiding random walk (57,58). These measurements highlighted the fact that smaller loops are much more stable than expected from entropic considerations alone, even for loops with lengths comparable to the statistical segment length. This enhanced stability of small loops was attributed to significant intraloop stacking interactions that decrease with increasing loop size, as indicated by the large value of the apparent exponent α (46,56).

To explain the slow folding times for hairpins, we proposed that the chain dynamics prior to the formation of the critical nucleus is slowed down as a result of intrachain interactions in the unfolded state that transiently trap the ss-chain in 'misfolded' conformations (30,46,59). These misfolded conformations could arise from mis-paired base-pairs, nonnative hydrogen bonding and intrastrand stacking interactions, as have been observed in large-scale, molecular dynamics simulations of RNA hairpin-folding trajectories (39,40,60). A 'roughness' in the free energy landscape is expected to increase the effective configurational diffusion time of the ss-chain (61,62). A similar roughness has been implicated to rationalize the experimentally obtained values of the characteristic diffusion coefficient in the end-to-end contact measurements in polypeptides, and the significant temperature dependence observed for this diffusion coefficient (63,64).

A satisfying confirmation of the idea that intrachain interactions in ss-polynucleotides slow down the diffusion of the chain configuration has come from direct measurements of the end-to-end contact formation, that demonstrated that contact formation in ss-chains with 4 nt in the loop occurs on time-scale ~400 ns–8 μs, not tens–of–nanoseconds (65). The ~10-fold difference that remains between the time-scales for end-to-end contact formation and hairpin closing times may be accounted for by an additional factor that takes into account local conformational fluctuations of the bases that bring them into the correct 'native' orientation for base-pairing to occur (66). This additional slowing down to form native contacts has been implicated (66) as a plausible explanation for the discrepancy between end-to-end contact times of ~10–300 ns for ~10-residues long polypeptides loops (63,64,67–69), and the much slower time-scales of β-hairpin formation, of ~6 μs (70).

No such systematic study of the stability and kinetics of RNA hairpins with varying loop sizes has been carried out to our knowledge. The sequence-dependent stability of small loops in ssDNA and RNA hairpins has been investigated in some detail by Bevilacqua and co-workers (71–75). Their measurements indicate a network of hydrogen bonds in the loop region, as well as interactions between the loop and the closing base pair, that contribute significantly to the stability of hairpins. Interestingly, they found that smaller loops in ssDNA, especially for tri- or tetra-loop sequences of the form GNA or GNAB, (N = A,C,G,T; B = C,G,T), with CG closing base-pair, fold much more cooperatively than small loops in RNA with a stable loop motif GNRA (R = A,G) (75). These studies raise the question as to whether there are fundamental differences in intraloop and loop–stem interactions in ssDNA and RNA hairpins.

Here, we have investigated the loop-size dependence of the stability and kinetics of formation of RNA hairpins. The RNA hairpins used for this study consisted of 5 bp in the stem and a loop size that was expanded from 4 to 34 nt by oligoU insertions. The thermodynamics and kinetics of the RNA hairpins, in 2.5 mM $MgCl_2$, revealed significantly less dependence of the hairpin stability on loop size, compared to previous measurements on ssDNA hairpins, which were carried out in 100 mM NaCl. Parallel experiments on ssDNA hairpins in 2.5 mM and 33.3 mM $MgCl_2$, however, showed that these differences are primarily due to the differences in the counterions. Thus, small poly(dT) loops and small poly(rU) loops are stabilized by similar mechanisms in ssDNA and RNA hairpins, respectively. The folding times for both ssDNA and RNA hairpins are found to scale with the length of the loops as $\sim L^{2.2-2.6}$, independent of the polynucleotide type, sequence, or kind of counterions used. Interestingly, this scaling behavior is similar to the length dependence observed for loop closure times in polypeptides (63,64,67), and is consistent with the idea that the rate-limiting step in the formation of hairpins is the entropic search in conformational space for the correct nucleation loop, albeit with an effectively smaller diffusion coefficient as a result of intrachain interactions.

MATERIALS AND METHODS

RNA hairpins

RNA oligomers were obtained from Dharmacon, with the sequences 5′-rCGAUCUU(U_j)CCGA*UCG-3′, with $j = 0$,

5, 15 and 30. For fluorescence experiments, 2-aminopurine (2AP) was substituted at the position marked with A*. Deprotected RNAs were purified by denaturing 20% polyacrylamide gel electrophoresis, concentrated by ultrafiltration (Centricon, Millipore) and desalted by several exchanges against 10 mM Tris–HCl, pH 7.5. DNA oligomers were obtained from Oligos Etc. (Wilsonville, OR, USA), with the sequences 5′-CGGATAA(T_N)TTAT CCG-3′, with $N = 4$, 8, 10, 12, 16, 20. The buffer used in all experiments with RNA hairpins was 10 mM Tris–HCl, pH 7.5, 2.5 mM $MgCl_2$. For ssDNA hairpins, the buffers were 10 mM sodium phosphate, pH 7.5, 100 mM NaCl, 0.1 mM EDTA or 10 mM Tris–HCl, pH 7.5, with either 2.5 mM or 33 mM $MgCl_2$. The strand concentrations for equilibrium and T-jump measurements were about 100 μM. A 5-fold dilution of samples did not produce any shift in the melting profiles within experimental error, indicating that all strands at concentration of 100 μM are sufficiently diluted to prevent bimolecular association.

Equilibrium measurements

The fluorescence spectra of the 2AP-labeled RNA hairpins were acquired for a range of temperatures between 15°C and 90°C, by measuring the static fluorescence spectra of 2AP between 315 and 450 nm, after excitation at 311 nm, using a Fluoromax-2 spectrofluorimeter (Jobin Yvon-Spex, Edison, NJ, USA). Optical melting profiles were obtained from the fluorescence emission maximum (at 368 nm) as a function of temperature. For the ssDNA hairpins, that did not contain 2AP, the melting profiles were obtained from absorbance measurements at 266 nm, using Hewlett Packard 8452A spectrophotometer (Palo Alto, CA, USA). The fluorescence (or absorbance) versus temperature profiles were normalized to obtain the fraction of molecules in the unfolded (or open) state, $f_U(T)$, by fitting the fluorescence (or absorbance) profiles $F(T)$ to a two-state transition plus an upper (F_U) and a lower (F_L) baseline: $F(T) = f_U(T)[F_U(T) - F_L(T)] + F_L(T)$. The upper and lower baselines were parameterized as straight lines with independently varying slopes. The fraction $f_U(T)$ was described in terms of a van't Hoff expression:

$$f_U(T) = \frac{1}{1 + \exp[-\Delta H_{vH}/R(1/T - 1/T_m)]} \quad \mathbf{1}$$

Here, ΔH_{vH} is the enthalpy of a fully intact hairpin relative to the unfolded state and is assumed, for simplicity, to be temperature independent, T_m is the melting temperature of the hairpin at which $f_U = 1/2$, and R is the gas constant. The equilibrium constant $K_{eq}(T)$ for each hairpin is obtained from the melting profiles as $K_{eq}(T) = (1 - f_U)/f_U$. The van't Hoff parameters for each of the hairpins in this study are summarized in Table 1.

Equation 1 assumes that the unfolding transition occurs without any significant changes in the heat capacity of the system. For a more accurate parameterization of the melting transition, the heat capacity changes should be explicitly included (76,77), and will affect primarily the enthalpy parameter ΔH_{vH}. The T_m that characterizes the midpoint of the transition, and which is used for further analysis, is essentially independent on whether the heat capacity is taken into account in Equation 1 or not, and is affected primarily by the accuracy with which the baselines can be determined.

Dependence of hairpin stability on loop size

In a two-state approximation the equilibrium constant $K_{eq} = \exp(-\Delta G_{hairpin}/RT)$, where $\Delta G_{hairpin}$ is the free energy of the hairpin relative to the unfolded state. Thus, writing $\Delta G_{hairpin} = \Delta G_{stem} + \Delta G_{loop}$, we have

$$\begin{aligned} K_{eq} &= \exp(-\Delta G_{stem}/RT)\exp(-\Delta G_{loop}/RT) \\ &= z_{stem}(N_s)z_{loop}(N) \end{aligned} \quad \mathbf{2}$$

where z_{stem} is the statistical weight of the stem, z_{loop} the statistical weight of the loop, N_s is the number of base-pairs in the stem and N is the number of bases in the loop. The loop contributions to the stability of the hairpin are written as:

$$z_{loop}(N) = z_{wlc}(N)\sigma_{loop}(N) \quad \mathbf{3}$$

where z_{wlc} is the end-loop weighting function from a wormlike chain description of the probability of loop formation with N bases in the loop:

$$z_{wlc}(N) = \left(\frac{3}{2\pi b^2}\right)^{3/2} V_r g(N) \quad \mathbf{4}$$

Here, $b = 2P$ is the statistical segment length (also known as the Kuhn's length) and P is the persistence length, V_r is a characteristic reaction volume within which the bases at the two ends of the loop can form hydrogen bonds, $g(N)$ is the loop-closure probability, which, for a wormlike chain model, is written as derived by Shimada and Yamakawa (78).

$$g(N) = \begin{cases} N_b^{-3/2}\left[1 - \dfrac{5}{8N_b} - \dfrac{79}{640N_b^2}\right], & N_b > 4 \\ 84.90N_b^{-5}\exp\left(-\dfrac{7.027}{N_b} + 0.492N_b\right), & N_b \le 4 \end{cases} \quad \mathbf{5}$$

where $N_b = (N + 1)h/b$ is the number of statistical segments in the loop, and h is the internucleotide distance. The expression for $g(N)$, for $N_b < 4$, differs from the one used in our prior publications (56), which was taken from an earlier work by Yamakawa and Stockmayer (79). As pointed out by Shimada and Yamakawa (78), the earlier calculation overestimated the loop-closure probability for small loops, with $N_b < 4$. The revised calculation of Shimada and Yamakawa (78) describes more accurately the loop-closure probabilities for small loops obtained by Monte Carlo simulations.

In Equation 3, $\sigma_{loop}(N)$ is a phenomenological parameterization of the experimental observation on several ssDNA hairpins that the strength of the stem–loop and/or intra-loop stacking interactions appear to increase with decreasing loop size (31,56), and is written as

$$\sigma_{loop}(N) = \langle\sigma\rangle^{1/2} + \frac{C_{loop}}{N_b^{\gamma}} \quad \mathbf{6}$$

where $\langle\sigma\rangle$ is the cooperativity parameter, and is taken to be equal to the average of the 10 different stacking interactions and assigned a value of 4.5×10^{-5} (80,81). Thus, for large loops, $\sigma_{\mathrm{loop}}(N)$ approaches $\langle\sigma\rangle^{1/2}$. C_{loop} parameterizes the contribution to hairpin stability from intraloop and loop–stem interactions, and γ parameterizes the dependence of this stabilizing term on loop size.

In the case of ssDNA hairpins, we follow our previous description of the statistical weight of the stem as

$$z_{\mathrm{stem}}(N_s) = \sigma_c \langle\sigma\rangle^{1/2} \left(\prod_{i=1}^{Ns} s_i \right) \quad \mathbf{7}$$

where s_i is the statistical weight corresponding to the i-th base-pair. The s_i depends on the type of base-pair and interactions with its neighbors, and includes contributions to a base-pair's stability from hydrogen bonding as well as stacking interactions, as described earlier (80). The s_{i} parameters have been determined for 100 mM NaCl (80). The additional parameter, σ_{c} (=1, in 100 mM NaCl), is a correction factor to parameterize the overall change in the stability of the stem in salt conditions other than 100 mM NaCl.

For RNA hairpins, the thermodynamic parameters for formation of the stem were obtained from nearest neighbor terms $\Delta H^{\circ}\frac{\mathrm{XY}}{xy}$ and $\Delta S^{\circ}\frac{\mathrm{XY}}{xy}$, which are the enthalpy and entropy changes, respectively, for forming two adjacent base-pairs: Xx stacked next to Yy (82,83). Since the published values for ΔH° and ΔS° were measured in 1 M NaCl, we use the parameter σ_{c} to account for the overall stability of RNA hairpins under our ionic conditions of 2.5 mM $MgCl_2$. This σ_{c} also accounts for any changes in the stem stability from 2AP base substitution. Previous measurements of the equilibrium melting profiles of ssDNA hairpins, with 2AP incorporated at various sites along the stem, have shown that 2AP substitution can lower the melting temperature by 5–10°C (30,56). The extent of the destabilization depends on the type of nucleotide located next to 2AP, suggesting that disruption in the nearest-neighbor stacking interactions is a contributing factor.

Thus, the statistical weight of the RNA stem is written as

$$z_{\mathrm{stem}} = \sigma_{\mathrm{c}} \exp(-\Delta H_{\mathrm{stem}}/RT) \exp(\Delta S_{\mathrm{stem}}/R) \quad \mathbf{8}$$

where ΔH_{stem} for our RNA hairpin (Figure 1) is given by

$$\Delta H_{\mathrm{stem}} = \Delta H^{\circ}\frac{\mathrm{CG}}{\mathrm{GC}} + \Delta H^{\circ}\frac{\mathrm{GA}}{\mathrm{CU}} + \Delta H^{\circ}\frac{\mathrm{AU}}{\mathrm{UA}} + \Delta H^{\circ}\frac{\mathrm{UC}}{\mathrm{AG}} = -44.9\ \mathrm{kcal/mol} \quad \mathbf{9}$$

Similarly, ΔS_{stem} for our RNA hairpin is given by (82,83)

$$\Delta \mathrm{S}_{\mathrm{stem}} = \Delta \mathrm{S}^{\circ}\frac{\mathrm{CG}}{\mathrm{GC}} + \Delta \mathrm{S}^{\circ}\frac{\mathrm{GA}}{\mathrm{CU}} + \Delta \mathrm{S}^{\circ}\frac{\mathrm{AU}}{\mathrm{UA}} + \Delta \mathrm{S}^{\circ}\frac{\mathrm{UC}}{\mathrm{AG}} = -118.4\ \mathrm{eu}. \quad \mathbf{10}$$

Each of the terms in Equations 9 and 10 were obtained from Table 4 of ref. (83).

The statistical weight of the loop, z_{loop}, is identical in form to that for ssDNA hairpins, as described in Equations 3–6. The persistence length P was assigned a value of 1 nm for both RNA and ssDNA strands in $MgCl_2$ solutions, which is close to the value of ~0.8 nm for poly(rU) strands from force-extension measurements carried out in 2.5 mM Mg^{2+} (K. Visscher, personal communication), and in 10 mM $MgCl_2$ with 50 mM KCl (84). In 100 mM monovalent salt, experimental measurements of the persistence length range from ~1.4 nm for ssDNA in 100 mM Cs^{+} (85) to ~1.7 nm for poly(dT) in 100 mM NaCl (86) to ~2.5 nm for poly(dT) in 100 mM NaCl (87). We assigned $P \approx 1.4$ nm in 100 mM NaCl to be consistent with our earlier study of the statistical mechanical description of hairpins with poly(dT) loops (31,56). h was assigned a value of 0.6 nm (88,89), and the reaction volume V_r was calculated with r = 1 nm (90). For each set of measurements corresponding to the dependence of T_{m} on loop size of RNA or DNA hairpins, the experimentally obtained T_{m} was compared with the calculated value of T_{m} for a given set of parameters, defined as the temperature for which $\Delta G_{\mathrm{hairpin}} = 0$ or $K_{\mathrm{eq}} = 1$ in Equation 2. The set of parameters for RNA or DNA hairpins were varied to minimize the residual sum-of-squares, as described in the following section.

The contribution of the free energy of loop formation to hairpin stability is calculated from the parameters obtained from the fit, as follows:

$$\Delta G_{\mathrm{loop}}(N) = -RT \ln\left[z_{\mathrm{loop}}(N)\right] = -RT \ln\left[z_{\mathrm{wlc}}(N)\left(\langle\sigma\rangle^{1/2} + C_{\mathrm{loop}}/N_b^{\gamma}\right)\right] \quad \mathbf{11}$$

Note that ΔG_{loop} calculated using Equation 11 differs from calculations in our prior publications by a constant offset (31,56). Previously, we had included in the ΔG_{loop} calculation the free energy of forming the first base pair to close the loop, as well as the additional cooperativity parameter $\langle\sigma\rangle^{1/2}$that appears in the free energy of the stem [Equation 7]. Thus, in our prior publications, we had $\Delta G_{\mathrm{loop}} = -RT \ln\left[z_{\mathrm{loop}}(N) s \langle\sigma\rangle^{1/2}\right]$, where s is the statistical weight for forming the first base pair. The two calculations differ by a constant offset of around ~4 kcal/mol for ssDNA in 100 mM NaCl.

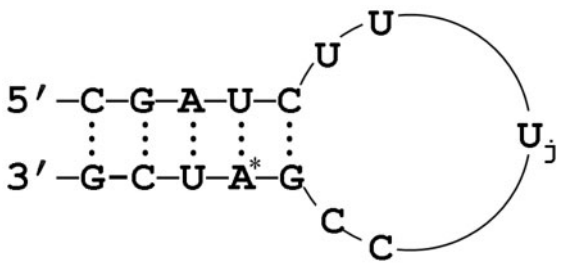

Figure 1. The RNA hairpin used in this study, with loop composition $UU(U_j)CC$, with j = 0, 5, 15 and 30. A* in the stem indicates the fluorescent analog 2AP instead of A.

Monte-Carlo procedure

Two parameters for ssDNA hairpins in 100 mM NaCl, C_{loop} and γ, and three parameters for ssDNA and RNA hairpins in 2.5 mM and 33.3 mM $MgCl_2$, σ_c, C_{loop} and γ were varied to best describe the dependence of the melting temperatures on the loop size. A simulated annealing procedure (91,92), based on that introduced by Metropolis *et al*. (93) was used to sample the parameter space in order to minimize the residual sum-of-squares, starting from 20 independent randomly chosen parameters from a plausible set of starting values.

Laser T-jump

Kinetics measurements on hairpin formation were carried out using a laser T-jump spectrometer, which consists of a multimode Q-switched Nd:YAG laser (Continuum Surelite II, 600 mJ/pulse at 1.06 μm, full width at half-maximum ≈ 6 ns) that is used to pump a 1-m long Raman cell containing high-pressure methane gas. The first Stokes line is separated from other wavelengths by a Pellin–Broca prism. The conversion efficiency at 1.54 μm measured after the prism was 10–15% yielding about 60–80 mJ/pulse. The 1.54 μm beam was focused down to about 1 mm (full width at half-maximum) on one side of the sample cuvette with 1 mm path length. A typical T-jump achieved with this configuration was about 10°C (30,31). The probe source was a 200-W Hg/Xe lamp with a 10 cm water filter and a 307 nm interference filter. The probe beam was focused down to a spot size of ~300 μm. The fluorescence from 2AP was filtered from background signal with a 365 nm interference filter, and detected by a photomultiplier tube (Hamamatsu R928) with a 5-MHz preamplifier (Hamamatsu C1053-51). The signal from the preamplifier was digitized using a 500-MHz transient digitizer (Hewlett Packard 54825A).

Analysis of kinetics measurements

The observed kinetics at each temperature were fit to the functional form $[I(\infty,T_f) - I(0^+,T_f)][1 - \exp(-k_r(T_f)t)] + I(0^+,T_f)$, where k_r is the relaxation rate coefficient, $I(\infty, T_f)$ is the equilibrium intensity of 2AP fluorescence at the final temperature T_f, and $I(0^+, T_f)$ is the intensity immediately after the laser pulse. $I(0^+, T_f)$ differs from the pre-T-jump baseline intensity $I(0^-, T_i)$ at the initial temperature T_i because of the intrinsic change in 2AP fluorescence with temperature. The initial temperature T_i of the sample was measured using a thermistor (YSI 44008, YSI, Yellow Springs, OH, USA) that was in direct contact with the sample holder. The final temperature T_f was determined by comparing the ratio $I(\infty, T_f)/I(0^-, T_i)$ with the equilibrium fluorescence versus temperature melting profile for each hairpin.

Analysis of temperature dependence of the relaxation time

The relaxation rates obtained from the single-exponential fit to the relaxation kinetics at each final temperature are the sum of the opening and closing rates: $k_r = k_o + k_c$. The equilibrium constant obtained from the melting profiles gives the ratio of the opening and closing rates: $K_{eq} = k_c/k_o$. Thus the opening ($\tau_o = 1/k_o$) and closing ($\tau_c = 1/k_c$) times were determined at each final temperature from the measured relaxation times $\tau_r = 1/k_r$ and K_{eq} as $\tau_o = \tau_r(1 + K_{eq})$ and $\tau_c = \tau_r(1 + 1/K_{eq})$. The temperature-dependence of the opening and closing times were fitted to the following set of Arrhenius equations, that include the viscosity dependence of the pre-exponential factor (33), to obtain the activation enthalpies $\Delta H_o^{\ddagger}$ and $\Delta H_c^{\ddagger}$ for the opening and closing steps, respectively:

$$\tau_o(T) = \tau_o(T_o)\frac{\eta(T)}{\eta_o(T_o)}\exp\left[\Delta H_o^{\ddagger}\left(\frac{1}{T} - \frac{1}{T_o}\right)\right]$$
$$\tau_c(T) = \tau_c(T_o)\frac{\eta(T)}{\eta_o(T_o)}\exp\left[\Delta H_c^{\ddagger}\left(\frac{1}{T} - \frac{1}{T_o}\right)\right] \quad 12$$

Estimate of uncertainties in parameters

In all cases, the uncertainty for each parameter was estimated by fixing it at different values and varying the other parameters in a least-squares fit. The uncertainties reflect a change in the residual sum-of-squares by a factor of 2. For the Monte Carlo fit of the T_m dependence on loop size in which three parameters were varied, σ_c and C_{loop} are coupled and not well determined. Thus, the uncertainties in these parameters are not reported. However, γ is well determined and less dependent on the particular choice of σ_c and C_{loop}. The uncertainties in γ were determined by systematically varying σ_c and C_{loop} such that the change in the residuals was within a factor of 2.

RESULTS AND DISCUSSION

Loop dependence of RNA hairpins

The RNA hairpin sequence used in this study was 5′-rCGAUCUU(U_j)CCGA*UCG-3′ (hairpin H1) with 5 bp in the stem, and the central UU(U_j)CC forming the loop (Figure 1). All measurements were carried out on four hairpins, denoted Y_4 ($j = 0$), Y_9 ($j = 5$), Y_{19} ($j = 15$) and Y_{34} ($j = 30$), where the subscript indicates the number of bases in the loop. A single adenine denoted by A* in the stem was substituted with the fluorescent base analog 2AP. The 2AP fluorescence emission decreases when the base is stacked in a double helix, allowing fluorescence detection of stem formation (94,95).

All equilibrium and kinetics measurements on these hairpins were carried out in 10 mM Tris–HCl, pH 7.5, 2.5 mM $MgCl_2$. For each of the hairpins, the fluorescence emission spectra of 2AP were measured as a function of temperature, in the wavelength range 315–450 nm, after excitation at 311 nm. The melting profiles, shown in Figure 2a, were obtained from the emission maximum at 368 nm. The normalized fluorescence (Figure 2b), obtained after subtracting the upper and lower baselines (as described in Materials and Methods section), was interpreted as the fraction of RNA hairpins that have melted. The melting temperatures obtained from this analysis (Table 1) were plotted as a function of the loop size in Figure 3a. As expected, the melting temperature decreased as the loop was expanded.

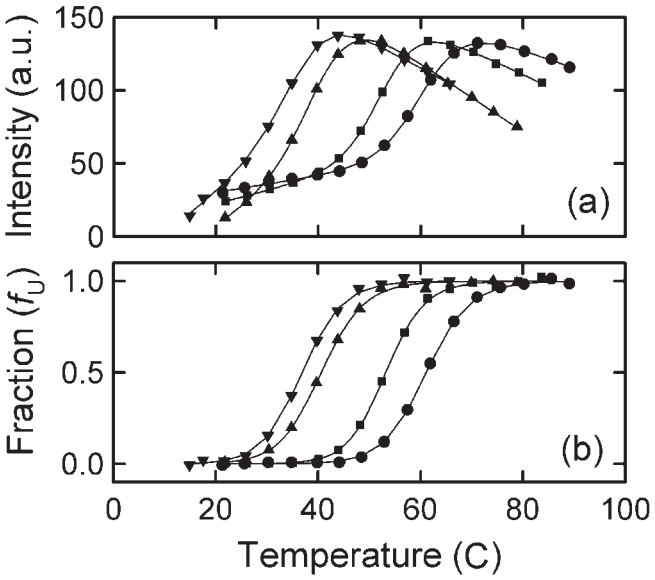

Figure 2. Fluorescence melting profiles for the RNA hairpin of Figure 1, with varying loop sizes, monitored with 2AP fluorescence. (**a**) The maximum of the fluorescence emission spectrum of 2AP, obtained at 368 nm, with excitation at 311 nm, is plotted as a function of temperature for hairpins Y_4 ($j = 0$: filled circle), Y_9 ($j = 5$: filled square), Y_{19} ($j = 15$: filled triangle) and Y_{34} ($j = 30$: inverted filled triangle). The symbols are the experimental data points. The continuous lines are calculated by fitting to a two-state van't Hoff analysis, as described in the text. The parameters describing the melting profiles are summarized in Table 1. (**b**) The normalized melting profiles, interpreted as the fraction of unfolded hairpins (f_U) for Y_4 (filled circle), Y_9 (filled square), Y_{19} (filled triangle) and Y_{34} (inverted filled triangle). The measurements were done in 2.5 mM $MgCl_2$ solution.

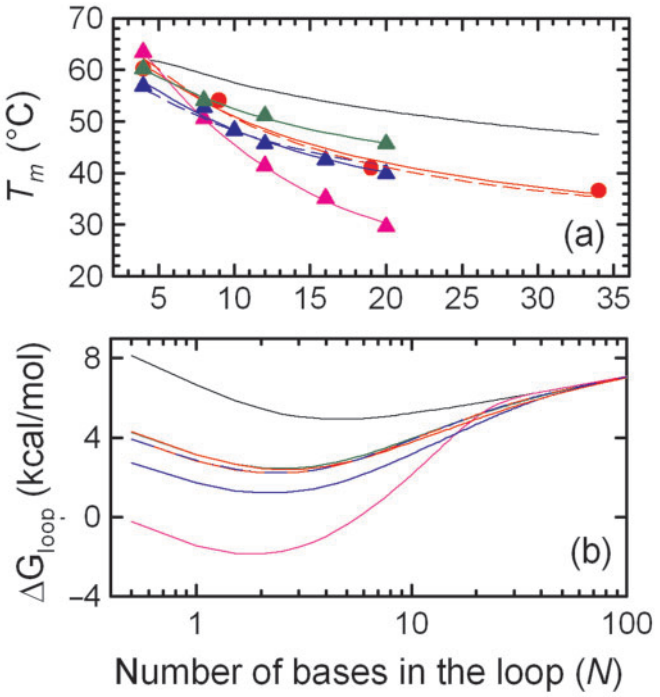

Figure 3. (**a**) The melting temperature (T_m) versus number of bases (N) in the loop of a fully intact hairpin. (filled red circle): RNA hairpins in 2.5 mM $MgCl_2$; (filled pink triangle): ssDNA hairpins in 100 mM NaCl; (filled blue triangle): ssDNA hairpins in 2.5 mM $MgCl_2$; (filled green triangle): ssDNA hairpins in 33 mM $MgCl_2$. The lines through the data points are the calculated T_m values at which the equilibrium constant K_{eq}, as defined in Equation 2, equals 1. The value of the persistence length used is 1 nm for RNA and ssDNA in $MgCl_2$, and 1.4 nm for ssDNA in 100 mM NaCl. The C_{loop}, γ, and σ_c parameters that best describe the loop-size dependence of T_m are summarized in Table 2. The continuous lines correspond to fits in which all the parameters are varied independently for each fit. The dashed lines for the data in 2.5 mM $MgCl_2$ correspond to the fit for which the C_{loop} and γ parameters are constrained to be the same for the ssDNA and RNA hairpins. The continuous black line represents the loop-size dependence for a hairpin for which the free energy of loop formation is close to the behavior expected for a semiflexible polymer, with a scaling exponent $\alpha \approx 2$. (**b**) The free energy of forming a loop with N bases in the loop, $\Delta G_{loop}(N)$, calculated using Equation 11 and the parameters C_{loop} and γ that best describe the data in Figure 3a., is plotted versus N for RNA in 2.5 mM $MgCl_2$ (red), ssDNA in 100 mM NaCl (pink), ssDNA in 2.5 mM $MgCl_2$ (blue) and ssDNA in 33.3 mM $MgCl_2$ (green). The continuous and dashed lines are as described for panel (a). The corresponding curve for a wormlike chain, calculated using Equation 11, with $C_{loop} = 0$, is shown in black.

In our earlier study on ssDNA hairpins, we used an equilibrium 'zipper' model in which we enumerated all microstates with partially melted stems to describe the equilibrium properties of these hairpins (30,31,56). This analysis showed that, at any temperature, the microstates that are primarily populated are either the intact hairpin or completely melted (56), suggesting that a two-state description of the thermodynamics of hairpin melting is adequate. Furthermore, despite recent evidence for a multi-step mechanism in the folding kinetics of ssDNA and RNA hairpins at temperatures far from T_m (28,34), the relaxation kinetics in response to a T-jump perturbation at temperatures near T_m are well described by a single-exponential decay. Therefore, in this article, we restrict all analysis of the thermodynamics and kinetics of ssDNA and RNA hairpins to a two-state system.

To describe the melting temperature as a function of the loop size, we write the free energy of the hairpin relative to the free energy of the melted (or unfolded) state as the sum of free energy terms for forming the stem and the loop [see Equation 2 in Materials and Methods section]: $\Delta G_{hairpin} = -RT \ln K_{eq} = -RT \ln\left(z_{stem}(N_s) z_{loop}(N)\right)$. The statistical weight of forming the loop, $z_{loop}(N)$, takes into account the probability of closing the loop assuming a semiflexible chain, and the base stacking interactions within the loop or between the loop and the stem [Equations 3–6]. The persistence length of the RNA strand was fixed at $P \approx 1$ nm. The statistical weight of the stem, $z_{stem}(N_s)$, is obtained from nearest neighbor parameters [Equation 8], with $\Delta H_{stem} = -44.9$ kcal/mol, $\Delta S_{stem} = -118.4$ eu, in 1 M NaCl. The parameter σ_c in Equation 8 corrects for changes in the stability of the stem in different salt conditions and from 2AP substitution.

In our model, the free energy of the hairpin is completely described by experimentally determined thermodynamic parameters for the hairpin stem, and three additional parameters that were varied to obtain the best fit to the data. The additional parameters were σ_c, C_{loop} and γ. As described in Materials and Methods section, C_{loop} parameterizes the strength of the intraloop and stem–loop interactions that contribute to the stability of

Table 1. van't Hoff parameters from melting profiles

Loop Size	RNA, 2.5 mM $MgCl_2$[a]		DNA, 2.5 mM $MgCl_2$[b]		DNA, 33.3 mM $MgCl_2$[b]		DNA, 100 mM NaCl[c]	
N	T_m, °C	ΔH_{vH}, kcal/mol	T_m, °C	ΔH_{vH}, kcal/mol	T_m, °C	ΔH_{vH}, kcal/mol	T_m, °C	ΔH_{vH}, kcal/mol
4	58.3	−56.2	–	–	60.2	−56.7	63.4	−40.8
8	–	–	52.7	−73.3	54.1	−65.9	50.5	−43.6
9	55.0	−42.6	–	–	–	–	–	–
10	–	–	48.3	−57.3	–	–	–	–
12	–	–	45.7	−68.4	51.1	−59.3	41.1	−42.8
16	–	–	42.5	−51.0	–	–	35.1	−61.5
19	41.3	−39.6	–	–	–	–	–	–
20	–	–	39.9	−69.1	45.7	−62.6	29.6	−58.3
34	36.2	−45.8	–	–	–	–	–	–

[a]From melting profiles data shown in Figure 2.
[b,c]Melting profiles not shown.
[c]from Shen *et al.* (31).
The uncertainty in T_m is ±1°C, and in ΔH is ±5 kcal/mol.

Table 2. Parameters obtained from fit to T_m versus loop size

	C_{loop}[a]	γ[b]	σ_c[a]
RNA, 2.5 mM $MgCl_2$	0.93	2.1	1.4×10^{-4}
RNA, 2.5 mM $MgCl_2$[c]	1.24	2.5	1.7×10^{-4}
DNA, 2.5 mM $MgCl_2$	6.42	2.9	8.40
DNA, 2.5 mM $MgCl_2$[c]	1.24	2.5	26.0
DNA, 33.3 mM $MgCl_2$	0.79	2.3	104
DNA, 100 mM NaCl	573	7.0	–

[a]The uncertainties in the parameters C_{loop} and σ_c are not well determined because the parameters are strongly coupled.
[b]The uncertainty in the γ values is ±0.5.
[c]The parameters were obtained by constraining the C_{loop} and γ parameters to be the same for the RNA and ssDNA hairpins.

the hairpin, and γ describes the deviation of the ΔG_{loop} dependence on the loop size from the dependence expected for an ideal semiflexible polymer. For loops of lengths (L) much greater than the statistical segment length, Equation 5 predicts that ΔG_{loop} for a random walk polymer will scale as $\sim\ln(L^{1.5})$. The additional dependence of hairpin stability on loop size expressed by γ in Equation 6 gives another factor of $\sim\ln(L^{\gamma})$ to the dependence of ΔG_{loop} on loop size. Thus, the experimentally observed dependence of hairpin stability on loop size is described by the apparent scaling exponent $\alpha \approx \gamma + 1.5$.

The T_m for each set of parameters was calculated as the temperature at which $\Delta G_{hairpin} = 0$. The parameters that best describe the dependence of the experimentally measured T_m on the number of bases N in the loop are summarized in Table 2 and the corresponding fit to the data is shown in Figure 3a. The best-fit parameters yield a value of $\gamma \approx 2.1$, which indicates that the free energy of RNA hairpins scale with loop size with an exponent of $\alpha \approx 3.6$.

Loop dependence of ssDNA hairpins

It is interesting to compare the results on the stability of RNA hairpins with varying loop sizes with our previous measurements on ssDNA hairpins, in which we investigated in detail the thermodynamics and kinetics of hairpins formed from the sequence 5′-dCGGATAA(X_N)TTATCCG-3′ (hairpin H2), with the number of bases in the loop varied from 4 to 12 for X = A,T (31,46,56,59). These measurements showed that the dependence of the stability of ssDNA hairpins scaled with the loop size with an apparent exponent α that ranged from ~6.9 to 8.3 for poly(dT) loops and $\alpha \approx 9.2$ for poly(dA) loops (31,56). Thus, for ssDNA hairpins, a semiflexible polymer description, which predicts $\alpha \approx 1.5$–2, was found to fail dramatically for loop sizes close to the optimal loop size of ~4 nt. These deviations were interpreted as arising from intra-loop and stem–loop interactions that stabilize hairpins with small loops (72,73,96,97), with the strength of these stabilizing interactions increasing with decreasing loop size (31,56).

RNA versus ssDNA loops

The results thus far on ssDNA and RNA hairpins suggest that the intra-loop interactions appear to be much weaker in RNA than in ssDNA. However, our earlier measurements on ssDNA hairpins were carried out in 100 mM NaCl, whereas the corresponding measurements on RNA hairpins were carried out in 2.5 mM $MgCl_2$. To determine whether the apparent difference in the behavior of the two polynucleotides is due to the difference in the salt conditions, we repeated the stability measurements on ssDNA hairpin H2 in 2.5 mM $MgCl_2$. As in the case of RNA hairpins, the free energy of the hairpin is described as in Equation 2, with z_{loop} still defined as in Equations 3–6 and z_{stem} defined as in Equation 7. The results of these measurements are also shown in Figure 3a for comparison, together with the results from previous measurements in 100 mM NaCl. The persistence lengths used in the fit are 1 nm for ssDNA strands in 2.5 mM $MgCl_2$ and 1.4 nm for ssDNA in 100 mM NaCl.

The most notable result from these measurements is that the dependence of T_m on loop size is essentially the same for ssDNA and RNA hairpins in 2.5 mM $MgCl_2$. The γ parameter for ssDNA hairpins in 2.5 mM Mg^{2+} is ~2.9 ($\alpha \approx 4.4$), close to $\gamma \sim 2.1$ ($\alpha \approx 3.6$) for RNA hairpins under identical salt conditions, and closer to $\alpha \approx 2$ expected from entropic considerations of loop formation for an ideal semi-flexible polymer. In contrast, reanalysis of our previous data on the same ssDNA hairpins in 100 mM NaCl, using a two-state description, shows strong

deviation from ideality, with $\gamma \approx 7$ ($\alpha \approx 8.5$), consistent with our previous analysis (31,56). All parameters obtained from the fits are summarized in Table 2.

Note that the T_m for RNA hairpin H1 and ssDNA hairpin H2 in different salt conditions are very similar for the hairpins with the smallest loop size, although the sequence and the length of the stems are quite different in the two hairpins. In particular, the RNA hairpin is closed by a CG base pair, which is known to stabilize hairpins relative to AT closing base pair (72,97,98). Furthermore, because intraloop interactions contribute to the stability of hairpins with small loops, any sequence- or salt-dependence of the intraloop interactions should give the largest variations in stability for small loops, as discussed subsequently. In contrast, we observe the largest deviation of T_m among large loops. The fact that the different sets of curves converge for small loops is probably accidental and likely reflects compensating differences in the stability of the RNA and DNA stems and loops in 100 mM NaCl and 2.5 mM $MgCl_2$. The observation that the stem stability is higher in 2.5 mM Mg^{2+} than in 100 mM Na^+ is consistent with previous measurements of the stabilizing effect of divalent cations on DNA and RNA duplexes (99,100).

The contribution of the loop to hairpin stability, and its dependence on loop-size, is best illustrated by a plot of ΔG_{loop} (N) versus loop size, calculated from Equation 11 (Figure 3b), which highlights the experimental observation that ssDNA hairpins with small loops are significantly more stable relative to hairpins with large loops, in 100 mM NaCl, in comparison with measurements in 2.5 mM $MgCl_2$ Thus, these results suggest that the intraloop interactions that contribute to the additional stability of small loops are diminished in the presence of low concentrations of divalent cations. The ΔG_{loop} (N) profiles also illustrate that these intraloop stabilizing interactions are very similar for ssDNA and RNA loops in 2.5 mM $MgCl_2$. An accurate estimate of the errors in the fit parameters is complicated by the fact that two of the three parameters, C_{loop}, which affects loop stability, and σ_c which affects the stem stability, are strongly coupled. An increase in C_{loop} can be compensated by a corresponding decrease in σ_c, with comparable residuals obtained from the fit to the data. The values of the γ parameter, on the other hand, were found to be relatively stable. To determine whether the loop parameters for ssDNA and RNA hairpins in 2.5 mM $MgCl_2$, and hence the corresponding ΔG_{loop} (N) dependence on loop size, are significantly different, or the same, to within the accuracy of our fitting procedure, we carried out a global fit to the T_m dependence on loop size for both hairpins in 2.5 mM $MgCl_2$, by constraining C_{loop} and γ to be identical for the two hairpins. The results of this fit are also shown in Figure 3, and the parameters yield a value of $\gamma \approx 2.5$ ($\alpha \approx 4$), and indicate that, within the noise in our T_m measurements, we cannot distinguish between the loop parameters for ssDNA and RNA hairpins. Thus, the contribution of intraloop interactions to loop stability, and the mechanism by which small poly(dT) loops in ssDNA hairpins are stabilized is very similar to that of poly(rU) loops in RNA hairpins, under identical salt conditions.

To exclude the possibility that the choice of our input parameters may be the reason for the large difference in the γ parameter obtained in NaCl versus $MgCl_2$, we examined the sensitivity of the γ parameter to changes in the value of the persistence length used in the fits. In the case of ssDNA at 100 mM NaCl, variations in the persistence length value from 1 to 2 nm gave values for the γ parameter in the range from ~6.4 to ~8.1. Persistence length values outside this range gave significantly worse residuals. We also examined the effect of introducing heat capacity changes (ΔC_p) in the description of the temperature-dependence of the statistical weights s_i in Equation 7. For ssDNA in 100 mM NaCl, the best fit, obtained with $P = 1.4$ nm and $\Delta C_p \approx 65$ cal/mol/K (76,77,101) gave $\gamma \approx 5.4$. For ssDNA in 2.5 mM $MgCl_2$, similar values of ΔC_p, with $P = 1$ nm, gave $\gamma \approx 2.0$. Thus, the γ-values obtained for ssDNA in 100 mM NaCl, which fall in the range of ~5.4–8.1, remain significantly larger than the γ-values obtained in $MgCl_2$ for both ssDNA and RNA hairpins, which fall in the range of 2.0–2.9.

A possible contribution to the observed values of γ may come from temperature-dependence of the persistence length, which is not included in the model presented here. Measurements of the radius of gyration of long poly(rA) and poly(rU) chains, from light scattering measurements, have indicated substantial temperature-dependence to the persistence length of poly(rA) chains, with more than a factor of 2 reduction in the radius of gyration observed between 0°C and 40°C (102), consistent with significant stacking of the adenine bases at low temperatures. In contrast, corresponding measurements in poly(rU) chains indicated a very weak temperature-dependence in the range 15–45°C (88). Both poly(rU) and poly(rA) chains of the same length were found to have similar dimensions at temperatures above 50°C, for which the poly(rA) chain is essentially unstacked. These results suggest that the persistence length of poly(dT) chains does not change significantly with temperature. Furthermore, our earlier observation that the γ-value for hairpins with poly(dA) loops is only slightly larger than for poly(dT) loops (31) suggests that any contribution to γ from changes in the persistence length with temperature must be small.

Relaxation time increases with RNA loop size

Relaxation kinetics in response to a laser T-jump perturbation were measured for each RNA hairpin over a temperature range close to the T_m for each sample. Typical relaxation kinetics obtained for each sample are shown in Figure 4. Each kinetics trace was fitted to a single-exponential decay to obtain the relaxation time τ_r. The results from kinetics measurements on all four hairpins as a function of temperature are summarized in Figure 5. The range of relaxation times observed depends quite dramatically on the size of the loop. For example, at the T_m of each of the hairpins, where the opening and closing times are identical, τ_r varies from ~10 μs for Y_4, to ~50 μs for Y_9 and ~500 μs for Y_{34}.

A more meaningful comparison is done by analyzing the loop-size dependence of the opening and closing times, τ_0 and τ_c, respectively, at a fixed temperature.

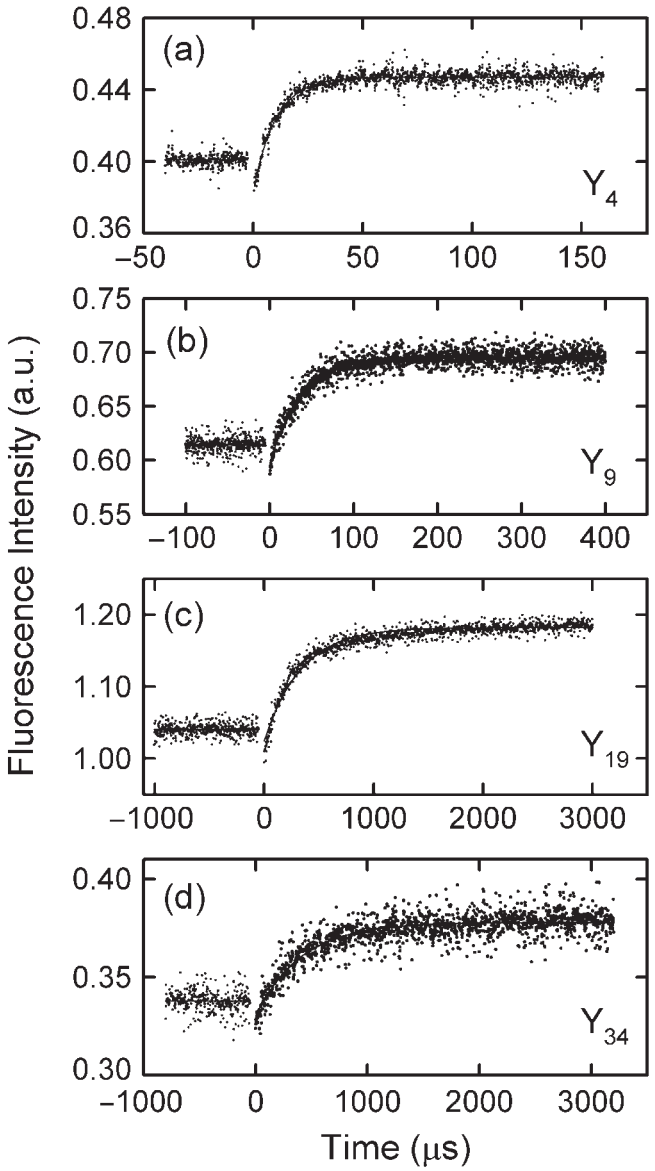

Figure 4. Relaxation kinetics for RNA hairpins monitored by measuring the change in fluorescence of 2AP at 365 nm after a laser T-jump. The fluorescence intensities at negative times correspond to 2AP fluorescence prior to the T-jump, at the initial temperature, T_i. The continuous lines through the relaxation kinetics correspond to single-exponential fits at the final temperature, T_f, with relaxation time τ_r. The kinetics shown are for (**a**) Y_4, with T-jump from 56.7°C to 60.0°C (τ_r = 10.3 μs), (**b**) Y_9, T-jump from 48.1°C to 50.2°C (τ_r = 36.3 μs), (**c**) Y_{19}, T-jump from 37.8°C to 40.1°C (τ_r = 334.2 μs) and (**d**) Y_{34}, T-jump from 33.6°C to 35.8°C (τ_r = 404.4 μs).

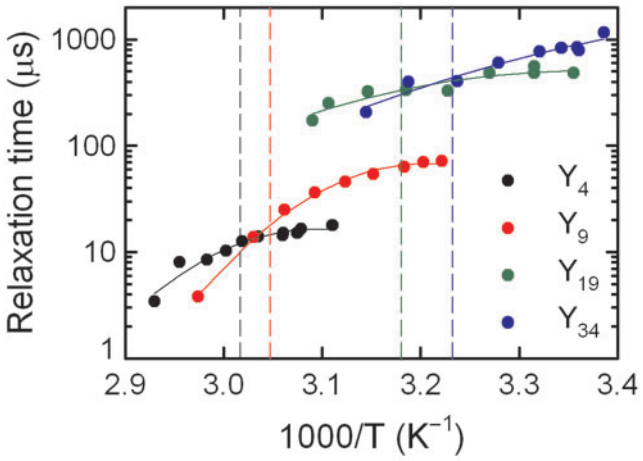

Figure 5. The measured relaxation times versus inverse temperature for RNA hairpins Y_4, Y_9, Y_{19} and Y_{34}. The relaxation times τ_r are obtained from single-exponential fits to the relaxation kinetics after a laser T-jump. The continuous lines are second-order polynomial fits to the data and are drawn to guide the eye. The melting temperature for each hairpin is indicated by the dashed vertical line.

The opening and closing times, for each of the RNA hairpins, obtained using a two-state analysis, with $\tau_0 = \tau_r(1 + K_{eq})$ and $\tau_c = \tau_r(1 + 1/K_{eq})$ at each final temperature, T_f, are summarized in Figure 6. Assuming Arrhenius behavior, we can obtain apparent activation enthalpies for the opening and closing steps, using Equation 12. The results from this analysis are summarized in Table 3. As observed in previous studies on the kinetics of DNA hairpins, the closing times are weakly dependent on temperature, with most of the temperature dependence observed in the opening times. These results indicate that the free energy barrier for the closing step is primarily entropic. Furthermore, in all cases with the exception of Y_9, the activation enthalpy for the closing step is negative, similar to what was observed in previous T-jump measurements on ssDNA hairpins (30,31,56). The opening and closing times exhibit slight deviations from a simple Arrhenius behavior, especially for hairpins with larger loops, which is attributed in part to heat capacity changes (76,77), and in part to a signature of misfolded transients in the folding kinetics (30,41,103).

We have interpreted the negative activation enthalpy for the closing step as indicative of a transition state ensemble that represents a nucleation intermediate consisting of microstates with one base pair formed to close the loop (30,46,56). This picture of the transition state is in concert with early work of Porschke and co-workers (21), who estimated the minimal size of the nucleus in an $A_6C_6U_6$ hairpin, as consisting of 3–4 A:U base-pairs, and is also in agreement with similar conclusions drawn by a detailed statistical mechanical model of hairpin folding (41). It should be noted that the negative activation enthalpy for the closing times obtained from the T-jump measurements are in contrast with FCS measurements on ssDNA hairpins, carried out mostly below T_m, that yielded positive activation enthalpies of ~5 kcal/mol for poly(dT) loops, and ~5–15 kcal/mol for poly(dA) loops (22,25,105). The origin of the differences between these measurements and interpretations were debated in a series of articles (25,31,59,104,105) and remain, to some extent, unresolved (46).

The dependencies of the opening and closing times on the length L of the loop ($L \sim N + 1$, where N is the number of bases in the loop) are shown in Figure 7. We picked 51°C as our reference temperature to facilitate comparison with the loop-dependence of the opening and closing times of ssDNA hairpins in 100 mM NaCl,

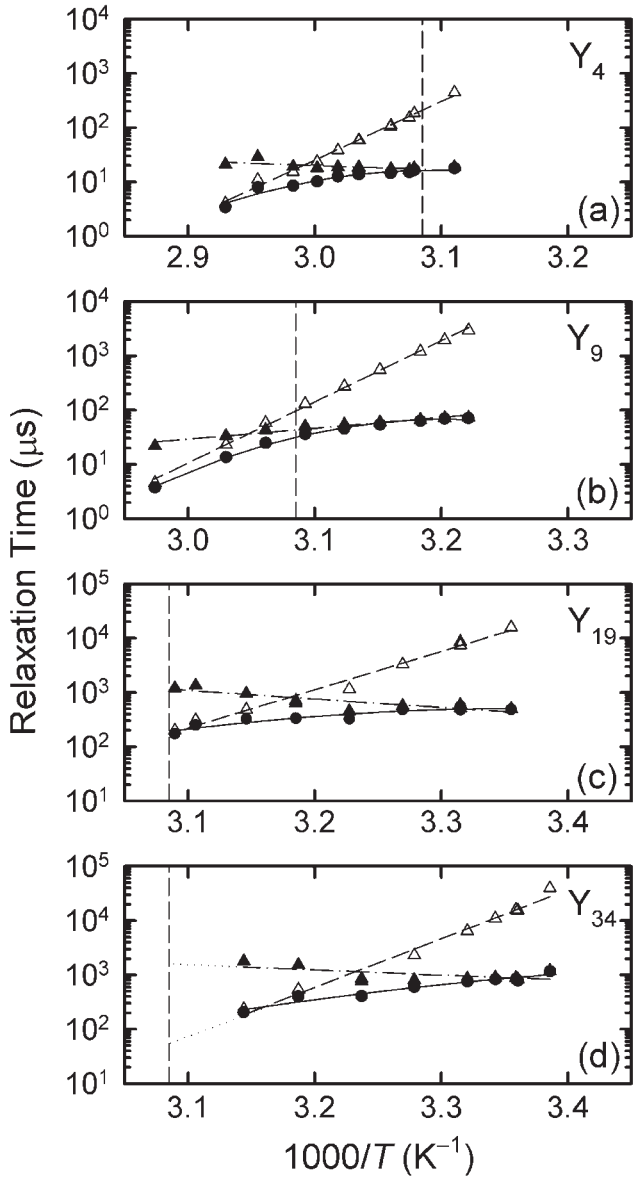

Figure 6. The measured relaxation times (τ_r), and the opening (τ_o) and closing (τ_c) times, versus inverse temperature for (**a**) Y_4, (**b**) Y_9, (**c**) Y_{19} and (**d**) Y_{34} RNA hairpins. τ_r (filled circle) are obtained from single-exponential fits to the relaxation kinetics; τ_o (open triangle) and τ_c (filled triangle) at each temperature are obtained from τ_r and K_{eq}, as described in the Materials and Methods section. The lines are from Arrhenius fits to the opening and closing times, using Equation 12, with the activation enthalpy for each step summarized in Table 3. The vertical lines are at 51°C, the temperature at which the loop-dependence of the opening and closing times is plotted in Figure 7.

obtained in an earlier study, and which was analyzed at ~51°C (31), as shown in Figure 7. Because of limited overlap in temperature for the four RNA hairpins that we measured, this requires extrapolation from the measured temperature dependence of the relaxation rates for only the hairpin Y_{34} (Figure 6). The closing times for the RNA hairpins scale with the loop size as $\sim L^{2.6\pm0.5}$ and for the ssDNA hairpins as $\sim L^{2.2\pm0.5}$ (Figure 7a). The data show that the closing times for both RNA and ssDNA hairpins are within a factor of 2 for all loop sizes, despite the

Table 3. Activation enthalpies for the opening and closing times[a]

Compound	$\Delta H_c^{\ddagger}$ kcal/mol	$\Delta H_o^{\ddagger}$ kcal/mol
Y_4	−7.0	46.0
Y_9	5.7	48.1
Y_{19}	−10.8	28.5
Y_{34}	−8.2	37.3

[a]The uncertainty in the activation enthalpy values is ±1 kcal/mol.

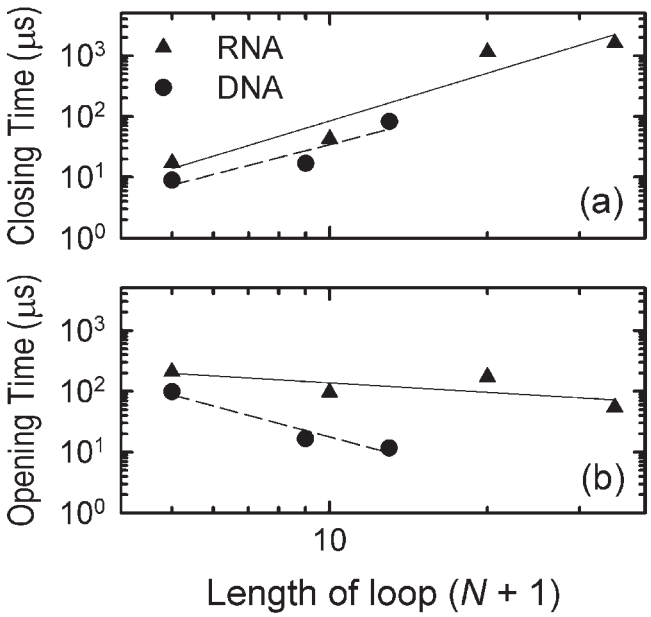

Figure 7. (**a**) The closing times and (**b**) the opening times versus the length of the loop $L\sim(N+1)$ for (filled triangle) RNA in 2.5 mM $MgCl_2$ and (filled circle) ssDNA hairpins in 100 mM NaCl, are plotted at $T \approx 51°C$. The lines are fits to the data using the functional form $\tau_c \sim (N+1)^{\nu}$ and $\tau_o \sim (N+1)^{-\beta}$, where $\nu = 2.6\pm0.5$ and $\beta = 0.5\pm0.2$ for RNA hairpins in 2.5 mM $MgCl_2$ and $\nu = 2.2\pm0.5$ and $\beta = 2.3\pm0.3$ for ssDNA hairpins in 100 mM NaCl.

differences in the stem sequence, the kind of counterions, and the temperature. More importantly, the scaling of the closing times with loop size is nearly identical for both hairpins under very different salt conditions. This scaling behavior is close to predictions from theory and simulations for the length dependence of loop closure time in random walk and semiflexible polymers, in the long chain limit (45,105–114). Thus, these results indicate that the loop dependence of the closing time is dominated by entropic search in conformational space for the correct nucleating state.

In contrast, all differences in the stability of the hairpins that are not from simple entropic considerations of loop formation appear in the opening times (Figure 7b). The opening times for ssDNA hairpins in 100 mM NaCl scale as $\sim L^{-2.3\pm0.3}$ (31), and for RNA hairpins in 2.5 mM $MgCl_2$ as $L^{-0.5\pm0.2}$. If we attribute all differences in the observed loop dependence in ssDNA and RNA hairpins on the different salt conditions, our kinetics results indicate a weaker loop-size dependence of the opening times in 2.5 mM $MgCl_2$.

In the context of the ideal semiflexible polymer model, with no intraloop interactions, the opening times are expected to be independent of the loop size. Deviations from this simple prediction are a direct consequence of the equilibrium measurements that show deviations in the scaling exponent α in comparison with semiflexible polymer models. These deviations in equilibrium measurements have to be reflected in the loop-size dependence of either the opening times or the closing times (or both). Our measurements show that the loop-size dependence of the closing times are in reasonable agreement with semiflexible polymer theories, and that most of the difference in the equilibrium constant shows up in the opening times. Thus, if the deviations in the equilibrium measurements are a result of intraloop stacking interactions, then these results suggest that in the transition state for the closing step, these intraloop interactions are not fully formed. In contrast, unfolding the hairpin requires disrupting the stem as well as the intraloop interactions. The weaker loop-size dependence of the opening times in 2.5 mM $MgCl_2$ is expected from the equilibrium measurements, because of the smaller discrepancy between the measured scaling exponent α and the value expected for a semiflexible polymer.

Our observation that the loop-size dependence of the closing times appears to be independent of the type of counterions is not inconsistent with recent theoretical predictions of the salt-dependence of loop-closure times for semiflexible polyelectrolytes (114). This study indicates that, for $[Na^+]$ above ~100 mM, the loop closure times are insensitive to the salt concentration. However, a dramatic increase in loop-closure times, especially for small loops ($L \approx 3P$) is predicted at $[Na^+] < 50$ mM, and remains to be investigated experimentally.

Effect of salt on the stability of small loops

Our equilibrium measurements reveal an unusual dependence of hairpin stability: hairpins with small loops are found to be less stable in the presence of 2.5 mM Mg^{2+} ions, than in the presence of 100 mM Na^+ ions. If electrostatic repulsion in small loops were to scale with the ionic strength in bulk solution, then we would expect this result, since the Debye screening length in 2.5 mM $MgCl_2$ is λ_D ~3.6 nm, in comparison with λ_D ~1 nm in 100 mM NaCl. This would suggest that the dependence of hairpin stability on loop size in ~100 mM NaCl would be similar to that in 33.3 mM $MgCl_2$, which also has λ_D ~1 nm (115). The results of these measurements are shown in Figure 3. The ssDNA hairpin stability curve in 33.3 mM $MgCl_2$ is much closer to the stability curves measured in 2.5 mM $MgCl_2$ ($\gamma \approx 2.3$), with most of the difference in hairpin stability observed between the two Mg^{2+} concentrations appearing in the stem contribution to the stability. The dependence of $\Delta G_{loop}(N)$ on loop size is found to be nearly identical for ssDNA hairpins in 2.5 mM and 33.3 mM $MgCl_2$. Thus, increasing the Mg^{2+} concentration above 2.5 mM did not affect the loop stability parameters. These results indicate that intraloop interactions that stabilize small loops are weaker in the presence of divalent ions relative to 100 mM NaCl, even when the ionic strengths of the bulk solution are matched and the predicted entropy changes due to localization of Na^+ or Mg^{2+} around the nucleic acid are similar (116).

An explanation for the unusual behavior of DNA and RNA molecules in the presence of low concentration of di- and multi-valent ions is offered by the counterion condensation theory that predicts that the local counterion concentration in the vicinity of the charged polymer will be almost independent of the bulk ion concentration (116–118). For multivalent ions in particular, condensation around the nucleic acid is strong, because of the lower entropic cost of localizing fewer ions. Condensation of counterions results in 75–90% charge neutralization in ssDNA and RNA even in millimolar Mg^{2+}, in comparison with only ~40% charge neutralization in 100 mM NaCl (116–118). Recent measurements on homopolymeric poly(rU) have demonstrated that at least 500 mM NaCl is needed to describe the force-extension curves with a wormlike chain model, in comparison with only 2.5 mM for $MgCl_2$ (55).

Extensive experiments have shown that multivalent ions play an important role in DNA condensation (119–123), as well as in the compaction and collapse transition of RNA molecules (124–128). In view of the counterion condensation theory, the role of the multivalent ions in stabilizing compact structures is thought to be primarily from attractive electrostatic interactions between negatively charged phosphate groups that have not been neutralized and residual positive charge on the localized multivalent ions (116–118). This may also be a contributing factor in the unusually small values of the persistence length for duplex DNA in the presence of low concentrations of multivalent cations in comparison with monovalent cations (129). For example, in the presence of ~2 mM Na^+ and 25 μM Mg^{2+}, the persistence length of duplex DNA is found to be slightly smaller (~40 nm) than the high monovalent salt (>100 mM Na^+) value of ~50 nm. In the presence of very low (few micromolar) $Co(NH_3)_6^{3+}$, the persistence length is further reduced to ~20–24 nm (130,131).

One explanation for the steep dependence of hairpin stability on loop size in 100 mM NaCl (Figure 3) is that, at these ion concentrations, the negative charge on the phosphates is not completely neutralized, and that, in the absence of any attractive interactions as in the case of multivalent ions, the ss chain is stiffer than predicted by the semiflexible polymer model, due to intrastrand charge repulsion. Thus, 100 mM NaCl could destabilize the unfolded (random coil) configuration to a larger extent than low concentrations of divalent ions, or, conversely, stabilize the folded conformations, and the magnitude of the difference between mono- and di-valent salts would depend on the size of the loop. This interpretation suggests that the hairpin folding times should also depend on salt, with hairpins in Mg^{2+} exhibiting slower folding times because of additional stability in the unfolded configurations (132). Our measurements show that the closing times for ssDNA in 100 mM NaCl and RNA in 2.5 mM $MgCl_2$, are very similar, with the latter being only slightly slower, within a factor of 2, for all loop sizes.

The observation that the closing times are very similar and exhibit nearly the same loop-size dependence under both salt conditions indicates that the lower stability of hairpins with small loops in the presence of divalent cations is not likely due to differences in the unfolded state in divalent and monovalent cations. An explanation that is more consistent with our equilibrium and kinetics measurements on ssDNA and RNA hairpins, in different salt conditions, is that smaller loops are significantly more stable in NaCl than in $MgCl_2$ as a result of specific interactions with Na^+ in the folded loop. This interpretation is supported by the observation that, in the absence of Na^+ ions, increasing the Mg^{2+} concentration from 2.5 mM to 33.3 mM did not affect the contribution of the loop stability, as measured by ΔG_{loop} (Figure 3b), to the stability of the hairpin.

CONCLUSION

Previous studies on the stability of ssDNA hairpins with different loop sizes have revealed that the free energy cost of loop formation deviates from the entropic cost estimated for a semiflexible polymer, with significant contribution to the stability from loop–stem and intraloop interactions (31,56,96,97). The strength of these intraloop interactions were found to *increase* dramatically for *smaller* loops (31,56). These measurements on ssDNA hairpins were carried out in 100 mM NaCl. Here, we have investigated the stability and folding kinetics of an RNA hairpin with poly(rU) loop of varying sizes, in 2.5 mM $MgCl_2$. For comparison, we also carried out stability measurements on ssDNA hairpins at different $MgCl_2$ concentrations. We find that the contribution of the free energy cost of loop formation, and its dependence on loop size, is nearly identical in ssDNA and RNA hairpins, under the same salt conditions. More interestingly, we find that the strength of the stabilizing intraloop interactions is diminished in 2.5 mM $MgCl_2$, such that the apparent loop-size dependence of hairpin stability is closer to that expected for an ideal semiflexible polymer. Furthermore, the free energy cost of loop formation does not change appreciably when Mg^{2+} concentration is increased from 2.5 to 33.3 mM. Thus, the largest effect on the changes in the stability of small loops is when Na^+ are replaced by Mg^{2+} ions.

The experimental observation that the dependence of the free energy cost of loop formation as a function of loop size in ssDNA and RNA chains, in the presence of low concentrations of Mg^{2+}, is closer to the behavior expected for an ideal semiflexible polymer, is consistent with recent observations on the effect of relatively low concentrations of divalent cations on the polymer properties of poly(rU) chains (55).

Interestingly, the closing times for RNA and ssDNA hairpins of varying loop sizes are found to be within a factor of 2, despite the differences in the stem sequence and the salt conditions. Furthermore, the scaling behavior of the closing times with loop size, for both ssDNA hairpins and RNA hairpins, is close to the scaling behavior expected for loop formation in semiflexible polymers, and independent of the salt conditions. These results reinforce the idea that the rate-determining step in the folding of hairpins is the entropic search in conformational space for the correct nucleating state.

Based on our equilibrium and kinetics measurements, a more plausible explanation for the increased loop stability in the presence of Na^+ ions versus Mg^{2+} ions, together with the apparent insensitivity of loop stability on the Mg^{2+} concentration, is that Na^+ ions interact specifically with the loop, and stabilize them. This effect is likely to be sequence dependent and needs further investigation. The role of Mg^{2+} in stabilizing tertiary RNA structures is well documented. Our observation that intraloop stacking interactions may be destabilized in the presence of Mg^{2+}, in comparison with Na^+, is an unexpected result that will have an impact on the discussion of the role of counterions in stabilizing folded structures in RNA.

ACKNOWLEDGEMENTS

We have benefited from helpful discussions with Dave Thirumalai and John Marko. This work was funded by National Science Foundation (MCB-0211254 and MCB-0721937 to A.A.); National Institutes of Health (GM60809 to S.A.W.) Funding to pay the Open Access publication charges for this article was provided by National Science Foundation grant MCB-0721937 to A.A.

Conflict of interest statement. None declared.

REFERENCES

1. Crews,S., Ojala,D., Posakony,J., Nishiguchi,J. and Attardi,G. (1979) Nucleotide sequence of a region of human mitochondrial DNA containing the precisely identified origin of replication. *Nature*, **277**, 192–198.
2. Roth,D.B., Menetski,J.P., Nakajima,P.B., Bosma,M.J. and Gellert,M. (1992) V(D)J recombination: broken DNA molecules with covalently sealed (hairpin) coding ends in scid mouse thymocytes. *Cell*, **70**, 983–991.
3. Gacy,A.M., Goellner,G., Juranic,N., Macura,S. and McMurray,C.T. (1995) Trinucleotide repeats that expand in human disease form hairpin structures *in vitro*. *Cell*, **81**, 533–540.
4. Wilson,K.S. and von Hippel,P.H. (1995) Transcription termination at intrinsic terminators: the role of the RNA hairpin. *Proc. Natl Acad. Sci. USA*, **92**, 8793–8797.
5. Glucksmann-Kuis,M.A., Dai,X., Markiewicz,P. and Rothman-Denes,L.B. (1996) E. coli SSB activates N4 virion RNA polymerase promoters by stabilizing a DNA hairpin required for promoter recognition. *Cell*, **84**, 147–154.
6. Uhlenbeck,O.C. (1990) Tetraloops and RNA folding. *Nature*, **346**, 613–614.
7. Cheong,C., Varani,G. and Tinoco,I.J. (1990) Solution structure of an unusually stable RNA hairpin, 5′GGAC(UUCG)GUCC. *Nature*, **346**, 680–682.
8. Heus,H.A. and Pardi,A. (1991) Structural features that give rise to the unusual stability of RNA hairpins containing GNRA loops. *Science*, **253**, 191–194.
9. Turner,D.H. and Sugimoto,N. (1988) RNA structure prediction. *Annu. Rev. Biophys. Biophys. Chem.*, **17**, 167–192.
10. Brion,P. and Westhof,E. (1997) Hierarchy and dynamics of RNA folding. *Annu. Rev. Biophys. Biomol. Struct.*, **26**, 113–137.
11. Tinoco,I. Jr. and Bustamante,C. (1999) How RNA folds. *J. Mol. Biol.*, **293**, 271–281.
12. Klausner,R.D., Rouault,T.A. and Harford,J.B. (1993) Regulating the fate of mRNA: the control of cellular iron metabolism. *Cell*, **72**, 19–28.

13. Draper,D.E. (1999) Themes in RNA-protein recognition. *J. Mol. Biol.*, **293**, 255–270.
14. Svoboda,P. and Cara,A.D. (2006) Hairpin RNA: a secondary structure of primary importance. *Cell Mol. Life. Sci.*, **63**, 901–908.
15. Winkler,W.C. and Breaker,R.R. (2005) Regulation of bacterial gene expression by riboswitches. *Annu. Rev. Microbiol.*, **59**, 487–517.
16. Dykxhoorn,D.M., Novina,C.D. and Sharp,P.A. (2003) Killing the messenger: short RNAs that silence gene expression. *Nat. Rev. Mol. Cell Biol.*, **4**, 457–467.
17. Cheng,J.C., Moore,T.B. and Sakamoto,K.M. (2003) RNA interference and human disease. *Mol. Genet. Metab.*, **80**, 121–128.
18. Cantor,C.R. and Schimmel,P.R. (1980) *Biophysical Chemistry Part III: The Behavior of Biological Macromolecules*. W. H. Freeman and Company, New York.
19. Coutts,S.M. (1971) Thermodynamics and kinetics of G-C base pairing in the isolated extra arm of serine-specific transfer RNA from yeast. *Biochim. Biophys. Acta*, **232**, 94–106.
20. Gralla,J. and Crothers,D.M. (1973) Free energy of imperfect nucleic acid helices. II. Small hairpin loops. *J. Mol. Biol.*, **73**, 497–511.
21. Porschke,D. (1974) Thermodynamics and kinetics parameters of an oligonucleotide hairpin helix. *Biophys. Chem.*, **1**, 381–386.
22. Bonnet,G., Krichevsky,O. and Libchaber,A. (1998) Kinetics of conformational fluctuations in DNA hairpin-loops. *Proc. Natl Acad. Sci. USA*, **95**, 8602–8606.
23. Deniz,A.A., Dahan,M., Grunwell,J.R., Ha,T., Faulhaber,A.E., Chemla,D.S., Weiss,S. and Schultz,P.G. (1999) Single-pair fluorescence resonance energy transfer on freely diffusing molecules: observation of Fèorster distance dependence and subpopulations. *Proc. Natl Acad. Sci. USA*, **96**, 3670–3675.
24. Wallace,M.I., Ying,L., Balasubramanian,S. and Klenerman,D. (2000) FRET fluctuation spectroscopy: exploring the conformational dynamics of a DNA hairpin loop. *J. Phys. Chem. B*, **104**, 11551–11555.
25. Goddard,N.L., Bonnet,G., Krichevsky,O. and Libchaber,A. (2000) Sequence dependent rigidity of single-stranded DNA. *Phys. Rev. Lett.*, **85**, 2400–2403.
26. Grunwell,J.R., Glass,J.L., Lacoste,T.D., Deniz,A.A., Chemla,D.S. and Schultz,P.G. (2001) Monitoring the conformational fluctuations of DNA hairpins using single-pair fluorescence resonance energy transfer. *J. Am. Chem. Soc.*, **123**, 4295–4303.
27. Jung,J. and Van Orden,A. (2005) Folding and unfolding kinetics of DNA hairpins in flowing solution by multiparameter fluorescence correlation spectroscopy. *J. Phys. Chem. B*, **109**, 3648–3657.
28. Jung,J. and Van Orden,A. (2006) A three-state mechanism for DNA hairpin folding characterized by multiparameter fluorescence fluctuation spectroscopy. *J. Am. Chem. Soc.*, **128**, 1240–1249.
29. Kim,J., Doose,S., Neuweiler,H. and Sauer,M. (2006) The initial step of DNA hairpin folding: a kinetic analysis using fluorescence correlation spectroscopy. *Nucleic Acids Res.*, **34**, 2516–2527.
30. Ansari,A., Kuznetsov,S.V. and Shen,Y. (2001) Configurational diffusion down a folding funnel describes the dynamics of DNA hairpins. *Proc. Natl Acad. Sci. USA*, **98**, 7771–7776.
31. Shen,Y., Kuznetsov,S.V. and Ansari,A. (2001) Loop dependence of the dynamics of DNA hairpins. *J. Phys. Chem. B*, **105**, 12202–12211.
32. Proctor,D.J., Ma,H., Kierzek,E., Kierzek,R., Gruebele,M. and Bevilacqua,P.C. (2004) Folding thermodynamics and kinetics of YNMG RNA hairpins: specific incorporation of 8-bromoguanosine leads to stabilization by enhancement of the folding rate. *Biochemistry*, **43**, 14004–14014.
33. Ansari,A. and Kuznetsov,S.V. (2005) Is hairpin formation in single-stranded polynucleotide diffusion-controlled? *J. Phys. Chem. B.*, **109**, 12982–12989.
34. Ma,H., Proctor,D.J., Kierzek,E., Kierzek,R., Bevilacqua,P.C. and Gruebele,M. (2006) Exploring the energy landscape of a small RNA hairpin. *J. Am. Chem. Soc.*, **128**, 1523–1530.
35. Liphardt,J., Onoa,B., Smith,S.B., Tinoco,I.J. and Bustamante,C. (2001) Reversible unfolding of single RNA molecules by mechanical force. *Science*, **292**, 733–737.
36. Onoa,B. and Tinoco,I. Jr. (2004) RNA folding and unfolding. *Curr. Opin. Struct. Biol.*, **14**, 374–379.
37. Woodside,M.T., Anthony,P.C., Behnke-Parks,W.M., Larizadeh,K., Herschlag,D. and Block,S.M. (2006) Direct measurement of the full, sequence-dependent folding landscape of a nucleic acid. *Science*, **314**, 1001–1004.
38. Woodside,M.T., Behnke-Parks,W.M., Larizadeh,K., Travers,K., Herschlag,D. and Block,S.M. (2006) Nanomechanical measurements of the sequence-dependent folding landscapes of single nucleic acid hairpins. *Proc. Natl Acad. Sci. USA*, **103**, 6190–6195.
39. Sorin,E.J., Engelhardt,M.A., Herschlag,D. and Pande,V.S. (2002) RNA simulations: probing hairpin unfolding and the dynamics of a GNRA tetraloop. *J. Mol. Biol.*, **317**, 493–506.
40. Sorin,E.J., Rhee,Y.M., Nakatani,B.J. and Pande,V.S. (2003) Insights into nucleic acid conformational dynamics from massively parallel stochastic simulations. *Biophys. J.*, **85**, 790–803.
41. Zhang,W. and Chen,S.J. (2002) RNA Hairpin Folding Kinetics. *Proc. Natl Acad. Sci. USA*, **99**, 1931–1936.
42. Zhang,W. and Chen,S.J. (2006) Exploring the complex folding kinetics of RNA hairpins: I. General folding kinetics analysis. *Biophys. J.*, **90**, 765–777.
43. Zhang,W. and Chen,S.J. (2006) Exploring the complex folding kinetics of RNA hairpins: II. Effect of sequence, length, and misfolded states. *Biophys. J.*, **90**, 778–787.
44. Hyeon,C. and Thirumalai,D. (2003) Can energy landscape roughness of proteins and RNA be measured by using mechanical unfolding experiments? *Proc. Natl Acad. Sci. USA*, **100**, 10249–10253.
45. Szabo,A., Schulten,K. and Schulten,Z. (1980) First passage time approach to diffusion controlled reactions. *J. Chem. Phys.*, **72**, 4350–4357.
46. Ansari,A. and Kuznetsov,S.V. (2004) Hairpin formation in polynucleotides: a simple folding problem? In Stroscio,M.A. and Dutta,M. (eds), *Biological Nanostructures and Applications of Nanostructures in Biology: Electrical, Mechanical & Optical Properties.*, Kluwer Academic Publishers, New York, pp 99–147.
47. Bustamante,C., Smith,S.B., Liphardt,J. and Smith,D. (2000) Single-molecule studies of DNA mechanics. *Curr. Opin. Struct. Biol.*, **10**, 279–285.
48. Maier,B., Bensimon,D. and Croquette,V. (2000) Replication by a single DNA polymerase of a stretched single-stranded DNA. *Proc. Natl Acad. Sci. USA*, **97**, 12002–12007.
49. Wuite,G.J., Smith,S.B., Young,M., Keller,D. and Bustamante,C. (2000) Single-molecule studies of the effect of template tension on T7 DNA polymerase activity. *Nature*, **404**, 103–106.
50. Gerland,U., Bundschuh,R. and Hwa,T. (2001) Force-induced denaturation of RNA. *Biophys. J.*, **81**, 1324–1332.
51. Montanari,A. and Mezard,M. (2001) Hairpin formation and elongation of biomolecules. *Phys. Rev. Lett.*, **86**, 2178–2181.
52. Zhang,Y., Zhou,H. and Ou-Yang,Z.C. (2001) Stretching single-stranded DNA: interplay of electrostatic, base-pairing, and base-pair stacking interactions. *Biophys. J.*, **81**, 1133–1143.
53. Dessinges,M.N., Maier,B., Zhang,Y., Peliti,M., Bensimon,D. and Croquette,V. (2002) Stretching single stranded DNA, a model polyelectrolyte. *Phys. Rev. Lett.*, **89**, 248102.
54. Cocco,S., Marko,J.F., Monasson,R., Sarkar,A. and Yan,J. (2003) Force-extension behavior of folding polymers. *Eur. Phys. J. E.*, **10**, 249–263.
55. Seol,Y., Skinner,G.M. and Visscher,K. (2004) Elastic properties of a single-stranded charged homopolymeric ribonucleotide. *Phys. Rev. Lett*, **93**, 118102.
56. Kuznetsov,S.V., Shen,Y., Benight,A.S. and Ansari,A. (2001) A semiflexible polymer model applied to loop formation in DNA hairpins. *Biophys. J.*, **81**, 2864–2875.
57. DeGennes,P.G. (1979) *Scaling Concepts in Polymer Physics*. Cornell University Press, Ithaca, N.Y.
58. Grosberg,A.Y. and Khokhlov,A.R. (1994) *Statistical Physics of Macromolecules*. AIP Press, New York.
59. Ansari,A., Shen,Y. and Kuznetsov,S.V. (2002) Misfolded loops decrease the effective rate of DNA hairpin formation. *Phys. Rev. Lett.*, **88**, 069801.
60. Sorin,E.J., Rhee,Y.M. and Pande,V.S. (2005) Does water play a structural role in the folding of small nucleic acids? *Biophys. J.*, **88**, 2516–2524.

61. Zwanzig,R. (1988) Diffusion in a rough potential. *Proc. Natl Acad. Sci. USA*, **85**, 2029–2030.
62. Bryngelson,J.D. and Wolynes,P.G. (1989) Intermediates and barrier crossing in a random energy model (with applications to protein folding). *J. Phys. Chem.*, **93**, 6902–6915.
63. Lapidus,L.J., Eaton,W.A. and Hofrichter,J. (2000) Measuring the rate of intramolecular contact formation in polypeptides. *Proc. Natl Acad. Sci. USA*, **97**, 7220–7225.
64. Buscaglia,M., Lapidus,L.J., Eaton,W.A. and Hofrichter,J. (2006) Effects of denaturants on the dynamics of loop formation in polypeptides. *Biophys. J.*, **91**, 276–288.
65. Wang,X. and Nau,W.M. (2004) Kinetics of end-to-end collision in short single-stranded nucleic acids. *J. Am. Chem. Soc.*, **126**, 808–813.
66. Zhou,H.-X. (2003) Theory for the rate of contact formation in a polymer chain with local conformational transitions. *J. Chem. Phys.*, **118**, 2010–2015.
67. Bieri,O., Wirz,J., Hellrung,B., Schutkowski,M., Drewello,M. and Kiefhaber,T. (1999) The speed limit for protein folding measured by triplet-triplet energy transfer. *Proc. Natl Acad. Sci. USA*, **96**, 9597–9601.
68. Hudgins,R.R., Huang,F., Gramlich,G. and Nau,W.M. (2002) A fluorescence-based method for direct measurement of submicrosecond intramolecular contact formation in biopolymers: an exploratory study with polypeptides. *J. Am. Chem. Soc.*, **124**, 556–564.
69. Fierz,B., Satzger,H., Root,C., Gilch,P., Zinth,W. and Kiefhaber,T. (2007) Loop formation in unfolded polypeptide chains on the picoseconds to microseconds time scale. *Proc. Natl Acad. Sci. USA*, **104**, 2163–2168.
70. Munoz,V., Thompson,P.A., Hofrichter,J. and Eaton,W.A. (1997) Folding dynamics and mechanism of beta-hairpin formation. *Nature*, **390**, 196–199.
71. Nakano,M., Moody,E.M., Liang,J. and Bevilacqua,P.C. (2002) Selection for thermodynamically stable DNA tetraloops using temperature gradient gel electrophoresis reveals four motifs: d(cGNNAg), d(cGNABg),d(cCNNGg), and d(gCNNGc). *Biochemistry*, **41**, 14281–14292.
72. Moody,E.M. and Bevilacqua,P.C. (2003) Thermodynamic coupling of the loop and stem in unusually stable DNA hairpins closed by CG base pairs. *J. Am. Chem. Soc.*, **125**, 2032–2033.
73. Moody,E.M. and Bevilacqua,P.C. (2003) Folding of a stable DNA motif involves a highly cooperative network of interactions. *J. Am. Chem. Soc.*, **125**, 16285–16293.
74. Moody,E.M. and Bevilacqua,P.C. (2004) Structural and energetic consequences of expanding a highly cooperative stable DNA hairpin loop. *J. Am. Chem. Soc.*, **126**, 9570–9577.
75. Moody,E.M., Feerrar,J.C. and Bevilacqua,P.C. (2004) Evidence that folding of an RNA tetraloop hairpin is less cooperative than its DNA counterpart. *Biochemistry*, **43**, 7992–7998.
76. Chalikian,T.V., Volker,J., Plum,G.E. and Breslauer,K.J. (1999) A more unified picture for the thermodynamics of nucleic acid duplex melting: a characterization by calorimetric and volumetric techniques. *Proc. Natl Acad. Sci. USA*, **96**, 7853–7858.
77. Rouzina,I. and Bloomfield,V.A. (1999) Heat capacity effects on the melting of DNA. 1. General aspects. *Biophys. J.*, **77**, 3242–3251.
78. Shimada,J. and Yamakawa,H. (1984) Ring-closure probabilities for twisted wormlike chains. Application to DNA. *Macromolecules*, **17**, 689–694.
79. Yamakawa,H. and Stockmayer,W.H. (1972) Statistical mechanics of wormlike chains. II. Excluded volume effect. *J. Chem. Phys.*, **57**, 2843–2854.
80. Wartell,R.M. and Benight,A.S. (1985) Thermal denaturation of DNA molecules: a comparison of theory with experiment. *Phys. Rep.*, **126**, 67–107.
81. Paner,T.M., Amaratunga,M., Doktycz,M.J. and Benight,A.S. (1990) Analysis of melting transitions of the DNA hairpins formed from the oligomer sequences d[GGATAC(X)4GTATCC] (X = A, T, G, C). *Biopolymers*, **29**, 1715–1734.
82. Serra,M.J. and Turner,D.H. (1995) Predicting thermodynamic properties of RNA. *Methods Enzymol.*, **259**, 242–261.
83. Xia,T., SantaLucia,J. Jr, Burkard,M.E., Kierzek,R., Schroeder,S.J., Jiao,X., Cox,C. and Turner,D.H. (1998) Thermodynamic parameters for an expanded nearest-neighbor model for formation of RNA duplexes with Watson-Crick base pairs. *Biochemistry*, **37**, 14719–14735.
84. Vanzi,F., Takagi,Y., Shuman,H., Cooperman,B.S. and Goldman,Y.E. (2005) Mechanical studies of single ribosome/mRNA complexes. *Biophys. J.*, **89**, 1909–1919.
85. Tinland,B., Pluen,A., Sturm,J. and Weill,G. (1997) Persistence length of single-stranded DNA. *Macromolecules*, **30**, 5763–5765.
86. Doose,S., Barsch,H. and Sauer,M. (2007) Polymer properties of polythymine as revealed by translational diffusion. *Biophys. J.*, **93**, 1224–1234.
87. Murphy,M.C., Rasnik,I., Cheng,W., Lohman,T.M. and Ha,T. (2004) Probing single-stranded DNA conformational flexibility using fluorescence spectroscopy. *Biophys. J.*, **86**, 2530–2537.
88. Inners,L.D. and Felsenfeld,G. (1970) Conformation of polyribouridylic acid in solution. *J. Mol. Biol.*, **50**, 373–389.
89. Mills,J.B., Vacano,E. and Hagerman,P.J. (1999) Flexibility of single-stranded DNA: use of gapped duplex helices to determine the persistence lengths of poly(dT) and poly(dA). *J. Mol. Biol.*, **285**, 245–257.
90. Friederich,M.W., Vacano,E. and Hagerman,P.J. (1998) Global flexibility of tertiary structure in RNA: yeast tRNAPhe as a model system. *Proc. Natl Acad. Sci. USA*, **95**, 3572–3577.
91. Kirkpatrick,S., Gelatt,C.D. and Vecchi,M.P. (1983) *Science*, **220**, 671–680.
92. Press,W.H., Flannery,B.P. and Teukolsky,S.A. (1986) *Numerical Recipes: The Art of Scientific Computing*. Cambridge University Press, Cambridge.
93. Metropolis,N., Rosenbluth,A.W., Rosenbluth,M.N., Teller,A.H. and Teller,E. (1953) Equation of state calculations by fast computing machines. *J. Chem. Phys.*, **21**, 1087–1092.
94. Ward,D.C., Reich,E. and Stryer,L. (1969) Fluorescence studies of nucleotides and polynucleotides. I. Formycin, 2-aminopurine riboside, 2,6-diaminopurine riboside, and their derivatives. *J. Biol. Chem.*, **244**, 1228–1237.
95. Rachofsky,E.L., Seibert,E., Stivers,J.T., Osman,R. and Ross,J.B. (2001) Conformation and dynamics of abasic sites in DNA investigated by time-resolved fluorescence of 2-aminopurine. *Biochemistry*, **40**, 957–967.
96. Hilbers,C.W., Haasnoot,C.A., de Bruin,S.H., Joordens,J.J., van der Marel,G.A. and van Boom,J.H. (1985) Hairpin formation in synthetic oligonucleotides. *Biochimie*, **67**, 685–695.
97. Vallone,P.M., Paner,T.M., Hilario,J., Lane,M.J., Faldasz,B.D. and Benight,A.S. (1999) Melting studies of short DNA hairpins: influence of loop sequence and adjoining base pair identity on hairpin thermodynamic stability. *Biopolymers*, **50**, 425–442.
98. Serra,M.J., Lyttle,M.H., Axenson,T.J., Schadt,C.A. and Turner,D.H. (1993) RNA hairpin loop stability depends on closing base pair. *Nucleic Acids Res.*, **21**, 3845–3849.
99. Nakano,S., Fujimoto,M., Hara,H. and Sugimoto,N. (1999) Nucleic acid duplex stability: influence of base composition on cation effects. *Nucleic Acids Res.*, **27**, 2957–2965.
100. Serra,M.J., Baird,J.D., Dale,T., Fey,B.L., Retatagos,K. and Westhof,E. (2002) Effects of magnesium ions on the stabilization of RNA oligomers of defined structures. *RNA*, **8**, 307–323.
101. Williams,M.C., Wenner,J.R., Rouzina,I. and Bloomfield,V.A. (2001) Entropy and heat capacity of DNA melting from temperature dependence of single molecule stretching. *Biophys. J.*, **80**, 1932–1939.
102. Eisenberg,H. and Felsenfeld,G. (1967) Studies of the temperature-dependent conformation and phase separation of polyriboadenylic acid solutions at neutral pH. *J. Mol. Biol.*, **30**, 17–37.
103. Wallace,M.I., Ying,L., Balasubramanian,S. and Klenerman,D. (2001) Non-Arrhenius kinetics for the loop closure of a DNA hairpin. *Proc. Natl Acad. Sci. USA*, **98**, 5584–5589.
104. Goddard,N.L., Bonnet,G., Krichevsky,O. and Libchaber,A. (2002) Goddard *et al.* reply. *Phys. Rev. Lett.*, **88**, 069802.
105. Aalberts,D.P., Parman,J.M. and Goddard,N.L. (2003) Single-strand stacking free energy from DNA beacon kinetics. *Biophys. J.*, **84**, 3212–3217.
106. Wilemski,G. and Fixman,M. (1974) Diffusion-controlled intrachain reactions of polymers. I. Theory. *J. Chem. Phys.*, **60**, 866–877.
107. Doi,M. and Edwards,S.F. (1986) *The Theory of Polymer Dynamics*. Clarendon Press, Oxford, U.K.

108. Friedman,B. and O'Shaughnessy,B. (1993) Theory of intramolecular reactions in polymeric liquids. *Macromolecules*, **26**, 4888–4898.
109. Pastor,R.W., Zwanzig,R. and Szabo,A. (1996) Diffusion limited first contact of the ends of a polymer: Comparison of theory with simulation. *J. Chem. Phys.*, **105**, 3878–3882.
110. Podtelezhnikov,A. and Vologodskii,A. (1997) Simulations of polymer cyclization by brownian dynamics. *Macromolecules*, **30**, 6668–6673.
111. Thirumalai,D. (1999) Time scales for the formation of the most probable tertiary contacts in proteins with applications to cytochrome *c*. *J. Phys. Chem. B*, **103**, 608–610.
112. Dua,A. and Cherayil,B.J. (2002) The dynamics of chain closure in semiflexible polymers. *J. Chem. Phys.*, **116**, 399–409.
113. Debnath,P. and Cherayil,B.J. (2004) Dynamics of chain closure: approximate treatment of nonlocal interactions. *J. Chem. Phys.*, **120**, 2482–2489.
114. Hyeon,C. and Thirumalai,D. (2006) Kinetics of interior loop formation in semiflexible chains. *J. Chem. Phys.*, **124**, 104905.
115. Israelachvili,J.N. (1992) *Intermolecular and Surface Forces, 2nd edn*. Academic Press, Harcourt Brace Jovanovich Publishers, London.
116. Bloomfield,V.A., Crothers,D.M. and Tinoco,I.J. (2000) *Nucleic Acids: Structures, Properties, and Functions*. University Science Books, Sausalito, CA.
117. Manning,G.S. (1978) The molecular theory of polyelectrolyte solutions with applications to the electrostatic properties of polynucleotides. *Q. Rev. Biophys.*, **11**, 179–246.
118. Record,M.T. Jr, Anderson,C.F. and Lohman,T.M. (1978) Thermodynamic analysis of ion effects on the binding and conformational equilibria of proteins and nucleic acids: the roles of ion association or release, screening, and ion effects on water activity. *Q. Rev. Biophys.*, **11**, 103–178.
119. Bloomfield,V.A. (1997) DNA condensation by multivalent cations. *Biopolymers*, **44**, 269–282.
120. Widom,J. and Baldwin,R.L. (1980) Cation-induced toroidal condensation of DNA studies with Co3+(NH3)6. *J. Mol. Biol.*, **144**, 431–453.
121. Widom,J. and Baldwin,R.L. (1983) Monomolecular condensation of lambda-DNA induced by cobalt hexamine. *Biopolymers*, **22**, 1595–1620.
122. Schellman,J.A. and Parthasarathy,N. (1984) X-ray diffraction studies on cation-collapsed DNA. *J. Mol. Biol.*, **175**, 313–329.
123. Ma,C. and Bloomfield,V.A. (1994) Condensation of supercoiled DNA induced by MnCl2. *Biophys. J.*, **67**, 1678–1681.
124. Russell,R., Millett,I.S., Doniach,S. and Herschlag,D. (2000) Small angle X-ray scattering reveals a compact intermediate in RNA folding. *Nat. Struct. Biol.*, **7**, 367–370.
125. Heilman-Miller,S.L., Thirumalai,D. and Woodson,S.A. (2001) Role of counterion condensation in folding of the Tetrahymena ribozyme. I. Equilibrium stabilization by cations. *J. Mol. Biol.*, **306**, 1157–1166.
126. Fang,X., Littrell,K., Yang,X.J., Henderson,S.J., Siefert,S., Thiyagarajan,P., Pan,T. and Sosnick,T.R. (2000) Mg2+-dependent compaction and folding of yeast tRNAPhe and the catalytic domain of the B. subtilis RNase P RNA determined by small-angle X-ray scattering. *Biochemistry*, **39**, 11107–11113.
127. Laing,L.G., Gluick,T.C. and Draper,D.E. (1994) Stabilization of RNA structure by Mg ions. Specific and non-specific effects. *J. Mol. Biol.*, **237**, 577–587.
128. Buchmueller,K.L., Webb,A.E., Richardson,D.A. and Weeks,K.M. (2000) A collapsed non-native RNA folding state. *Nat. Struct. Biol.*, **7**, 362–366.
129. Manning,G.S. (2006) The persistence length of DNA is reached from the persistence length of its null isomer through an internal electrostatic stretching force. *Biophys. J.*, **91**, 3607–3616.
130. Porschke,D. (1986) Structure and dynamics of double helices in solution: modes of DNA bending. *J. Biomol. Struct. Dyn.*, **4**, 373–389.
131. Baumann,C.G., Smith,S.B., Bloomfield,V.A. and Bustamante,C. (1997) Ionic effects on the elasticity of single DNA molecules. *Proc. Natl Acad. Sci. USA*, **94**, 6185–6190.
132. Heilman-Miller,S.L., Pan,J., Thirumalai,D. and Woodson,S.A. (2001) Role of counterion condensation in folding of the Tetrahymena ribozyme. II. Counterion-dependence of folding kinetics. *J. Mol. Biol.*, **309**, 57–68.